

Illustration of SIR for CETB

David Long, BYU

Version 1.1

3 Apr 2015 (last revised 11 Jan 2016)

Abstract

This brief report illustrates how the SIR algorithm works using actual SSM/I data. The results are visually compared to AVE and non-enhanced gridded (GRD) images.

1 Scatterometer Image Reconstruction (SIR) Radiometer Version

The Scatterometer Image Reconstruction (SIR) algorithm was developed to generate high resolution backscatter images from noisy scatterometer data. Since scatterometer data is typically imaged in dB, the original SIR algorithm included a non-linear log scaling step in the algorithm (Long et al., 1993). For application to radiometer data, the algorithm is converted to operate in linear (temperature) space (Long and Daum, 1998).

The SIR algorithm enables a tradeoff between noise and signal enhancement via the number of iterations. When the measurement SNR is high, the algorithm can be iterated until the signal is completely reconstructed. However, in the presence of noise, it is best to truncate the iteration before the algorithm terminates to avoid over enhancement of the noise (Early and Long, 2001). This results in only partial reconstruction of the signal. By selecting the optimum number of iterations, the overall error (signal+noise) is minimized, resulting high resolution estimates of the surface brightness temperature.

1.1 Signal Reconstruction and SIR

In the reconstruction/signal processing approach, $T_B(x,y)$ is treated as a noisy two-dimensional signal to be estimated from the measurements T_i . For practical reasons, $T_B(x,y)$ is treated as a discrete signal sampled at the map pixel spacing. This spacing must be set sufficiently fine so that the generalized sampling requirements (Gröchenig, 1992) are met for the signal and the measurements (Early and Long, 2001). Typically, this is one-fourth to one-tenth the size of antenna footprint size.

Let $T_B[x,y]$ be the discretely sampled surface brightness temperature we are attempting to estimate. For convenience we vectorize this two-dimensional signal over an N_x by N_y pixel grid into a single dimensional variable a_j where

$$a_j = T_B[x_l, y_k]$$

Equation 1

with $j=l+N_x k$. In terms of the discrete MRF, the sampled measurement equation can be written as (Long, 2015; D.G. Long and M.J. Brodzik, 2016)

$$T_i = \sum_{j \in \text{image}} h_{ij} a_j$$

Equation 2

where $h_{ij} = R(x_l, y_k; \phi_i)$ is the discrete MRF for the i th measurement evaluated at the j th pixel center and the summation is over the image. We require that the discrete MRF be normalized so that

$$1 = \sum_{j \in \text{image}} h_{ij}$$

Equation 3

In practice, the MRF is negligible some distance from the measurement so this sum need only be computed over an area local to the measurement position. Some care has to be taken near image boundaries.

For the collection of available measurements, Eq. 2 can be written as the matrix equation

$$\vec{T} = \mathbf{H}\vec{a}$$

Equation 4

where \mathbf{H} contains the sampled MRF for each measurement. Note that \mathbf{H} is (very) large, sparse, and may be overdetermined or underdetermined.

Estimating the brightness temperature at high resolution is equivalent to inverting Eq. 4. While a variety of approaches to this have been proposed, in practice, due to the large size of \mathbf{H} , iterative methods are used. One advantage of an iterative method is that regularization can be easily implemented by prematurely terminating the iteration; otherwise an explicit regularization method can be used.

The radiometer form of the Scatterometer Image Reconstruction (SIR) is a particular implementation of an iterative solution to Eq. 4 that has proven effective in generating high resolution brightness temperature images (Long and Daum, 1998). The SIR estimate approximates a maximum-entropy solution to an underdetermined equation and least-squares to an overdetermined system. The first iteration of SIR is termed AVE, and can be a useful estimate of the surface T_B of its own. The AVE estimate of the j th pixel is given by

$$a_j = \frac{\sum h_{ij} T_i}{\sum h_{ij}}$$

Equation 5

where the sums are over all measurements that have non-negligible MRF at the pixel. A minimum threshold (typically about -9dBi) is used to determine the definition “non-negligible”.

Later iterations of SIR are computed using the following iterative algorithm where the j th pixel value at the k th iteration is represented by p_j^k

$$f_i^k = \frac{1}{q_i} \frac{\sum h_{ij} p_j^k}{\sum h_{ij}}$$

Equation 6

$$q_i = \sum h_{ij}$$

Equation 7

where the sums are over the pixels in the image. The scale factor is computed as

$$d_i^k = \sqrt{T_i / f_i^k}$$

Equation 8

with the non-linear update term computed according to

$$u_{ij}^k = \begin{cases} \left[\frac{1}{2f_i^k} \left(1 - \frac{1}{d_i^k} \right) + \frac{1}{p_j^k d_i^k} \right]^{-1}, & d_i^k \geq 1 \\ \left[\frac{1}{2} f_i^k (1 - d_i^k) + p_j^k d_i^k \right], & d_i^k < 1 \end{cases}$$

Equation 9

This is a sigmoid compression term that helps minimize the impact of noise on the updated image value.

Once the entire set of measurements have been processed, the pixel estimates are updated according to,

$$p_j^{k+1} = \frac{1}{g_j} \sum h_{ij} u_{ij}^k$$

Equation 10

$$g_j = \sum h_{ij}$$

Equation 7

where the sums over i are over the number of available measurements. This process is iterated N times where N is selected to tradeoff noise and resolution, typically using simulation, see Long (2015).

2 Case Study

To illustrate the application of SIR and compare it to AVE and drop-in-the-bucket low-resolution grid (GRD) images, some numerical and image examples are provided. Because it use forward spatial projections, SIR cannot be computed for a single pixel, but requires computation over a large area. To avoid edge effects, we select a large region to compute the image, but only analyze the data over a smaller region contained within the larger region. (Edge effects result when part of the SRF falls outside the processing window.) A small study region was arbitrarily selected with a small-scale feature.

Figure 1 helps place the study area in its larger context. SSM/I H-pol 85 GHz channel data is used. The region is selected from the Northern Hemisphere were two orbits overlap not too far from the pole. The values near the outer rim of the area should not be considered too closely due to edge effects. Instead we focus on the smaller area contained within the blue box. Note that both AVE and SIR provide much finer spatial information than the GRD image. Black squares in the GRD image are the results of coverage gaps in the 85 GHz channel used.

Figures 2-4 shows GRD, AVE, and SIR images where the SIR image of the subarea where the SIR image is a particular iteration number. Again, note the improved resolution of AVE and SIR compared to GRD. Also note the better definition of edges and deeper nulls and peaks in SIR compared to AVE. The pixel resolution is 3.125 km for AVE and SIR and 25 km for GRD.

Figure 5 illustrates SIR images for different iteration numbers. Note that first iteration is AVE. As the iteration increases, the SIR images have more and more detail, but also increasing noise. Based on simulation results described in a separate report we will stop between 10 and 20 iterations. Continuing to 50 iterations subjectively appears to make the images too noisy.

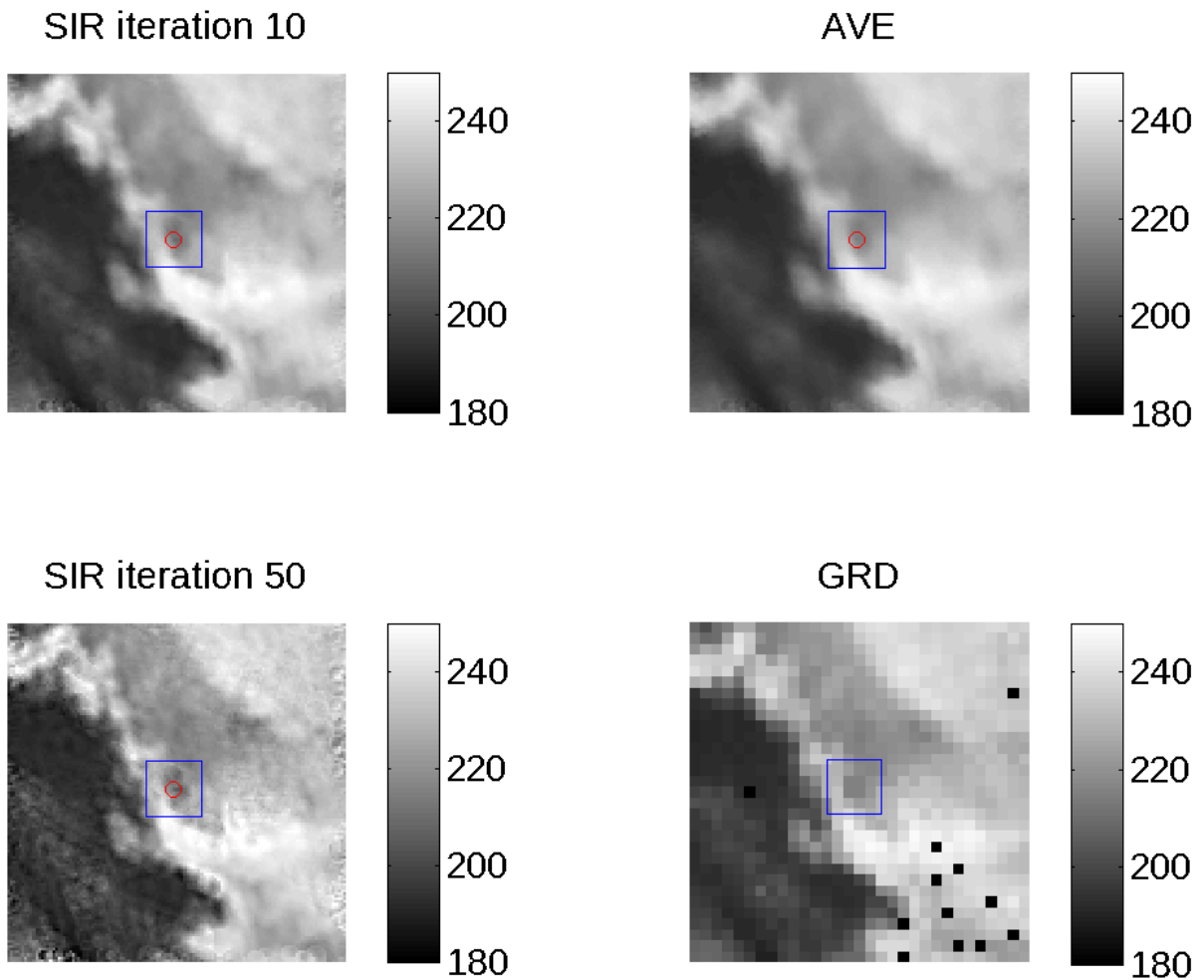


Figure 1. Regional context for study area (in blue box). AVE, GRD, and SIR images for two different iteration numbers are shown. The red circle shows the location of the single pixel study point. Black squares in the GRD image are pixels containing the centers of no measurements. Edge artifacts in the large SIR images are the result of the limited size of the context area shown, and will not affect full-sized product images.

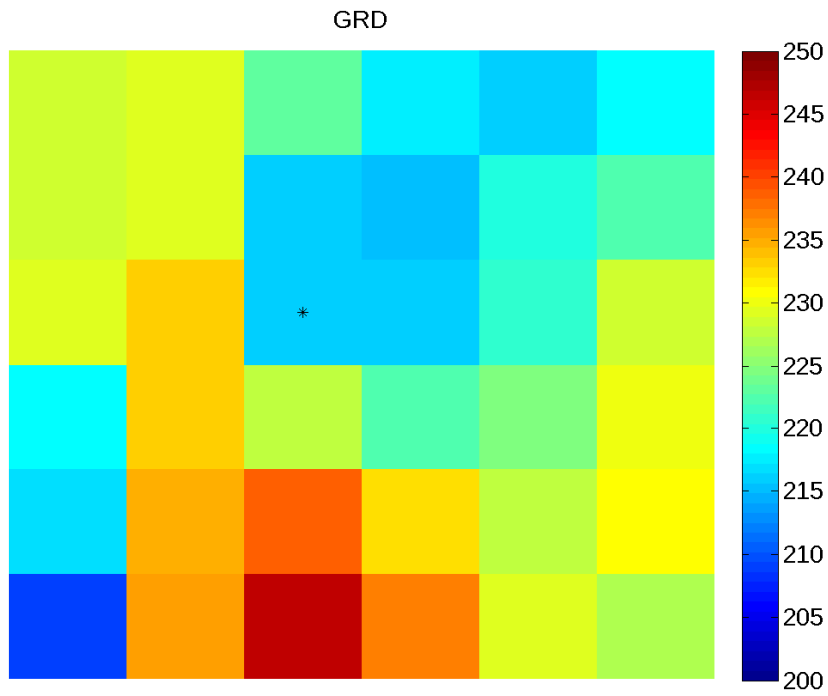


Figure 2. GRD image of study region. Compare Figs 3 and 4.

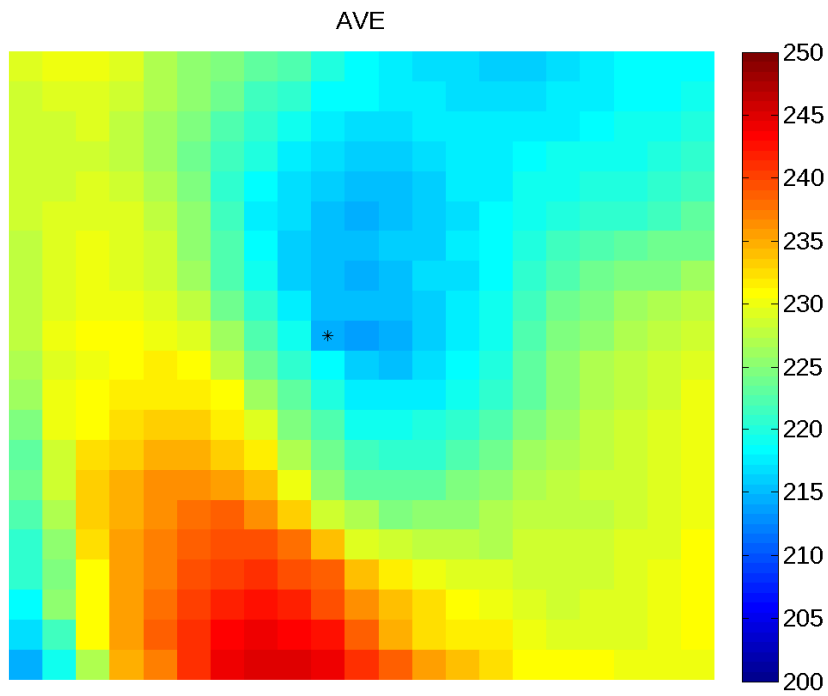


Figure 3. AVE image of study region. Compare Figs. 2 and 3.

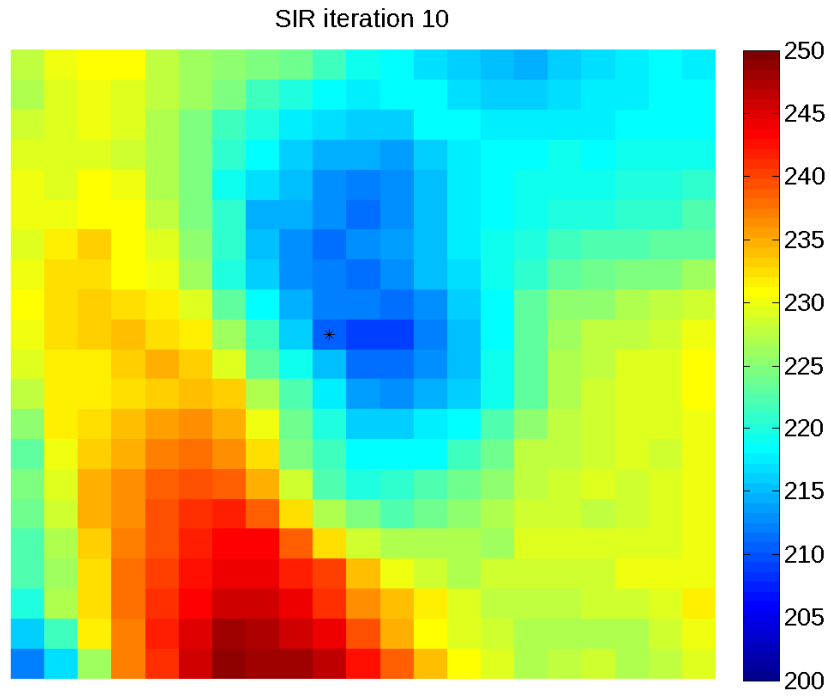


Figure 4. SIR image of study region for iteration 10. Compare Figs 2 and 3.

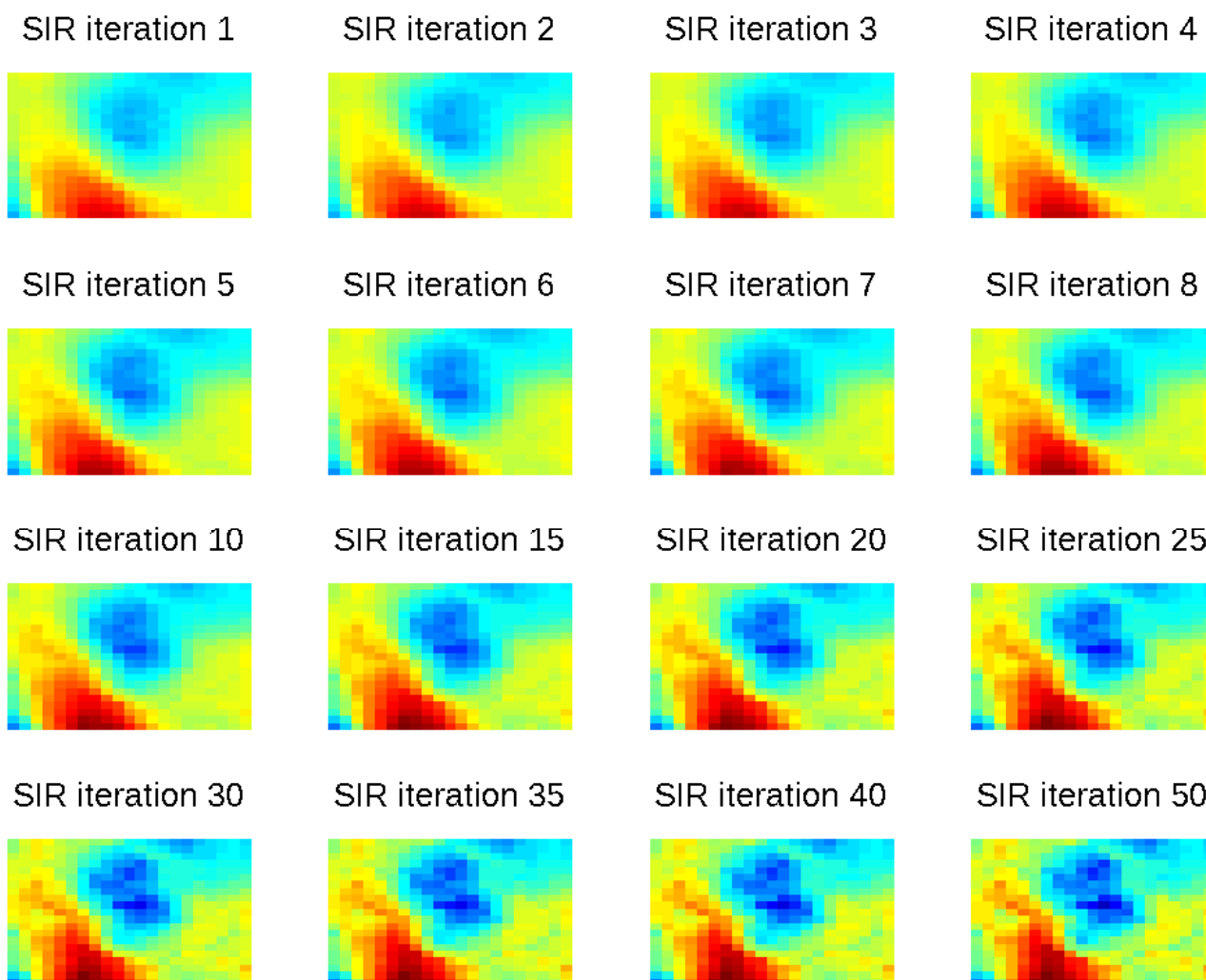


Figure 5. SIR image versus iteration

Figure 6 shows a plot of the value of the SIR pixel at a particular study point in the center of the image versus SIR iteration. Figure 7 shows the relative displacement of the measurements combined in AVE into the center pixel value. The relative weight of each pixel is also indicated. Note that the SIR estimate value will initially depend on these same pixels, but due to the use of feedback from the projection error from nearby measurements, the SIR pixel value depends on nearby pixels. The longer the iteration, the wider the region of influence on the pixel value. Figure 8 shows the SRF patterns for each of the measurements that overlap the central pixel.

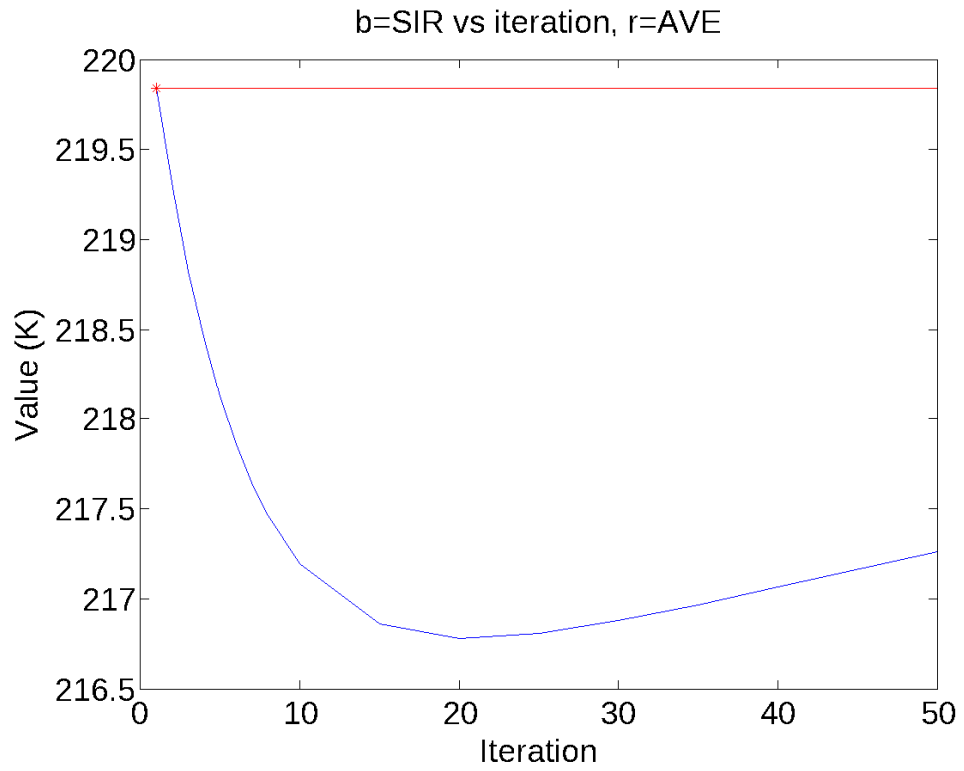


Figure 6. Value of pixel at the center of the study region versus SIR iteration.
Note that in the range 10-30 the pixel value is essentially constant.

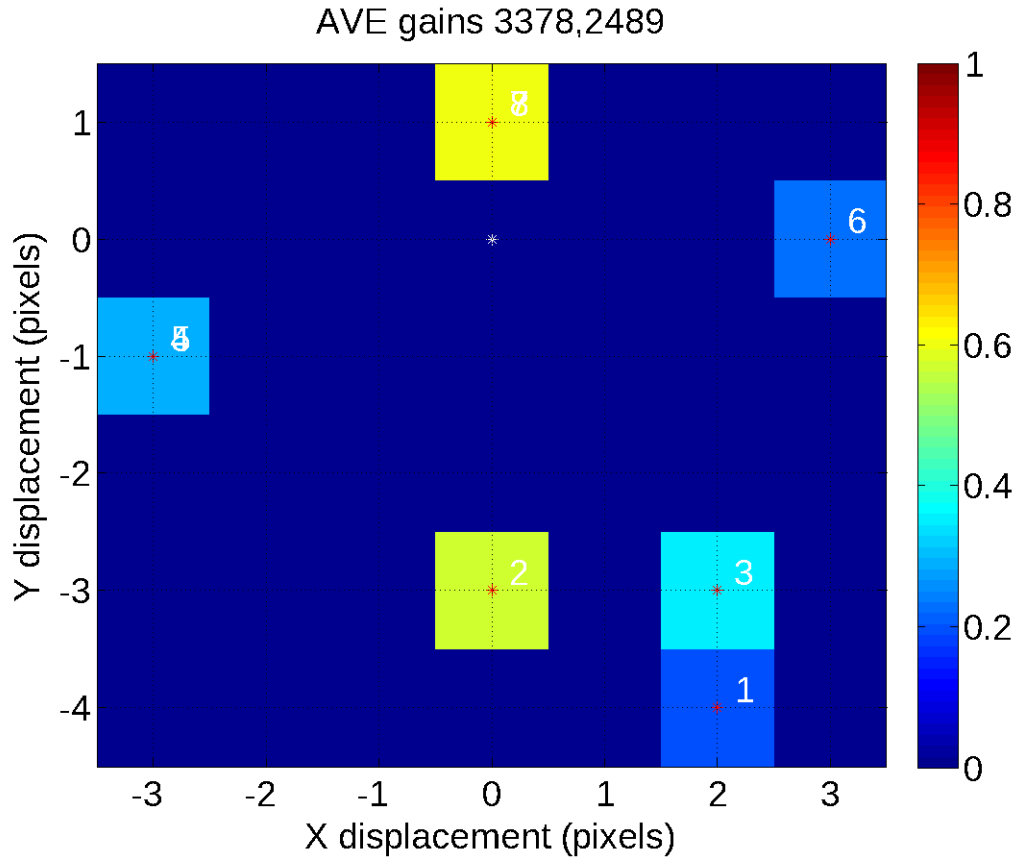


Figure 7. Relative displacements and AVE algorithm gains for each measurement that “touches” the center pixel of the study region.

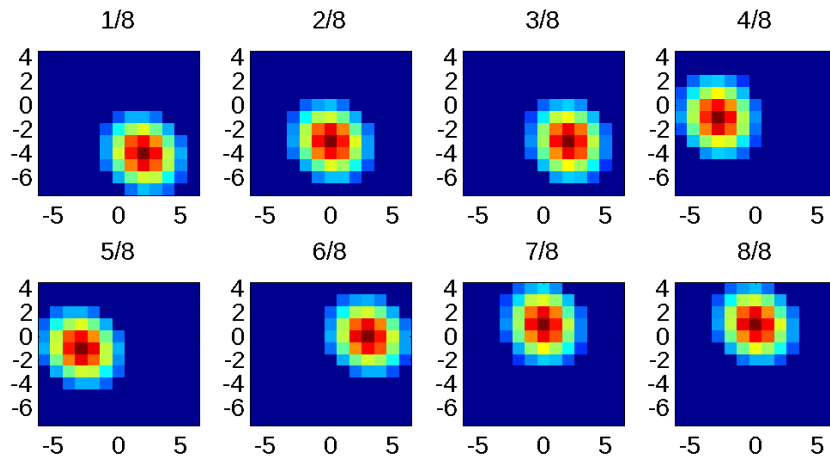


Figure 8. SRF patterns for each measurement in Fig. 6. Note that unlike BGI, measurements at the same location are not a concern for SIR and AVE.

3 Conclusion

This report has very briefly illustrated the difference between GRD, AVE, and SIR using actual SSM/I data. The improved resolution of SIR over GRD is readily apparent. Similarly, while AVE has better resolution than GRD, SIR has further improved resolution.

4 References

Early, D.S., and D.G. Long, Image Reconstruction and Enhanced Resolution Imaging from Irregular Samples, *IEEE Transactions on Geoscience and Remote Sensing*, Vol. 39, No. 2, pp. 291-302, 2001.

Long, D.G., P. Hardin, and P. Whiting, 1993. Resolution Enhancement of Spaceborne Scatterometer Data, *IEEE Transactions on Geoscience and Remote Sensing*, Vol. 31, No. 3, pp. 700-715.

Long, D.G., and D.L. Daum, 1998. Spatial Resolution Enhancement of SSM/I Data, *IEEE Transactions on Geoscience and Remote Sensing*, Vol. 36, No. 2, pp. 407-417.

Long, D.G., 2015. "Selection of Reconstruction Parameters (for the CETB Project)," National Snow and Ice Data Center (NSIDC) publication [Online] Available at: (http://nsidc.org/pmesdr/files/2015/04/Long_20150316_Resolution_Enhancement_Trade_offs.v3.3.pdf).

D.G. Long and M.J. Brodzik, 2016. Optimum Image Formation for Spaceborne Microwave Radiometer Products, *IEEE Transactions on Geoscience and Remote Sensing*, to appear, doi:10.1109/TGARS.2015.2505677.